PCCP

Accepted Manuscript

ROYAL SOCIETY OF CHEMISTRY

www.rsc.org/pccp

Physical Chemistry Chemical Physics
CREATED USING THE RSC LaTeX PCCP ARTICLE TEMPLATE – SEE www.rsc.org/electronicfiles FOR DETAILS
ARTICLE TYPE
www. rsc.org/xxxxxx | XXXXXXXX

First and second deprotonation of H_2SO_4 on wet hydroxylated (0001) α-quartz†

Garold Murdachaew,*[a] Marie-Pierre Gaigeot,[b,c] Lauri Halonen,[a] and R. Benny Gerber[a,d,e]

Received Xth XXXXXXXXXX 20XX, Accepted Xth XXXXXXXXX 20XX
First published on the web Xth XXXXXXXXXX 20XX
DOI: 10.1039/b000000x

We present an *ab initio* molecular dynamics study of deprotonation of sulfuric acid on wet quartz, a topic of atmospheric interest. The process is preferred, with 65% of our trajectories at 250 K showing deprotonation. The time distribution of the deprotonation events shows an exponential behavior and predicts an average deprotonation time of a few picoseconds. The process is exoergic, with most of the temperature increase being due to formation of hydrogen bonds prior to deprotonation. In agreement with existing studies of H_2SO_4 in water clusters, in liquid water, and at the air-water interface, the main determinant of deprotonation is the degree of solvation of H_2SO_4 by neighboring water molecules. However, we find that if both hydrogens of H_2SO_4 are simultaneously donated to water oxygens, deprotonation is disfavored. Predicted spectroscopic signatures showing the presence of solvated hydronium and bisulfate are presented. Increasing the temperature up to 330 K accelerates the process but does not change the main features of the deprotonation mechanisms or the spectroscopic signatures. The second deprotonation of H_2SO_4, studied only at 250 K, occurs provided there is sufficient solvation of the bisulfate by additional water molecules. In comparison to HCl deprotonation on the identical surface examined in our previous work, the first deprotonation of H_2SO_4 occurs more readily and releases more energy.

August 28, 2014

TOC Graphic

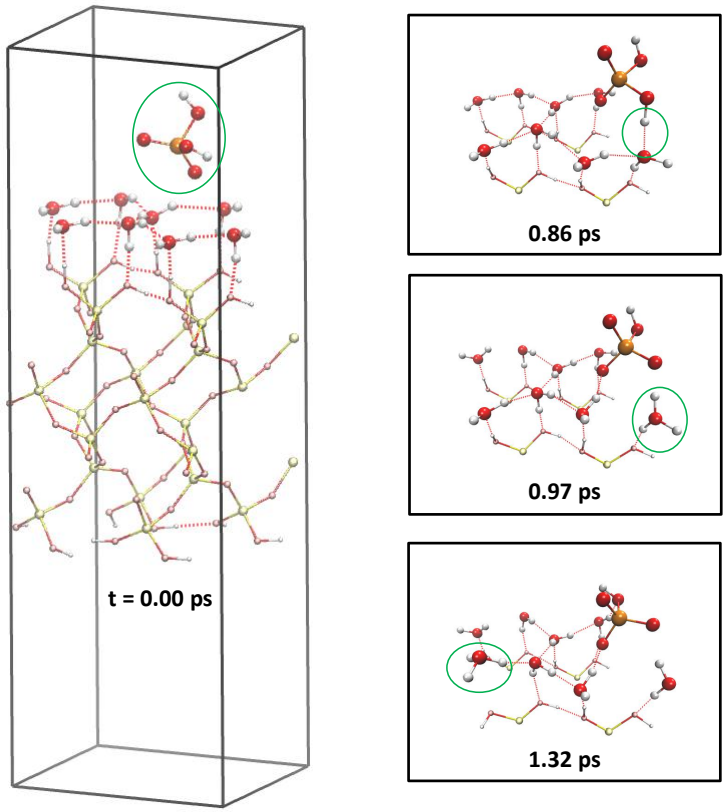

† Electronic Supplementary Information (ESI) available: Details of the quartz surface model, validation of the theory level used, trajectories, temperature effects (on deprotonation rate, mechanisms, and spectroscopic signatures), disordering of the water layer, and low energy configurations and bonding motifs of H_2SO_4 on wet quartz can be found in the ESI. See DOI: 10.1039/b000000x/

[a] *Laboratory of Physical Chemistry, Department of Chemistry, University of Helsinki, P.O. Box 55, FI-00014 Helsinki, Finland. Tel: +358 29 415 0291; E-mail: garold.murdachaew@helsinki.fi*
[b] *LAMBE, CNRS UMR 8587, Université d'Evry val d'Essonne, Boulevard François Mitterrand, Bâtiment Maupertuis, 91025 Evry, France.*
[c] *Institut Universitaire de France, 103 Boulevard Saint-Michel, 75005 Paris, France.*
[d] *Institute of Chemistry and the Fritz Haber Research Center, The Hebrew University, 91904 Jerusalem, Israel.*
[e] *Department of Chemistry, University of California, Irvine, California 92697, United States.*

1 Introduction

Sulfuric acid and related sulfur-containing molecules play important roles both technologically and in the natural environment[1,2] and participate in the biogeochemical sulfur cycle. Molecules such as OCS and SO_2 can be produced by natural processes (biological activity in marine organisms and volcanism, respectively) or anthropogenically (SO_2 from combustion of sulfur-containing fossil fuels). In the troposphere, in the presence of oxidants and/or humidity, sulfate species are quickly oxidized and/or hydrolyzed into H_2SO_4, a major component of acid rain and also a critical element in new particle formation.[3] Such particles may in turn act as cloud condensation nuclei (CCN), and the resulting clouds and sulfur-containing ice particles may contribute to increased rain fall and ozone depletion in polar stratospheric clouds, respectively. The net negative radiative forcing due to increased albedo of the sulfur-containing aerosols will lead to cooling.[4] This effect has motivated geoengineering proposals to counter a warming climate.[5,6] In addition to atmospheric chemistry, the uptake and possible reaction of acids on environmental interfaces is of interest to fields such as heterogeneous catalysis, sensor science, corrosion science, and cultural heritage science.[7]

H_2SO_4 is a strong diprotic acid and readily gives up a single proton, forming bisulfate, HSO_4^-. Further solvation can allow full deprotonation resulting in sulfate, SO_4^{2-}. A bulk water solution at 298 K has acid dissociation constants of $pK_{a1} = -3$ and $pK_{a2} = 1.99$. Only at high concentration, greater than 14 M, will H_2SO_4 remain in neutral form.[8] H_2SO_4 dissociation has been extensively studied both experimentally and theoretically in water clusters, in bulk liquid water, and at the air-water interface. Some examples of experimental and theoretical studies follow. Raman spectroscopy has been used to study the dissociation in bulk liquid water.[9] At the air-liquid interface and for surface studies, vibrational surface-sensitive spectroscopies such as VSFG (vibrational sum-frequency generation) have been employed both experimentally[10–18] and through theoretical modeling.[13–15] Finally, the process has also been studied at the air-water interface with photoelectron spectroscopy.[8] Research questions include the structure of the air-liquid interface and determining the balance between (partially) dissociated and undissociated sulfuric acid as a function of its concentration and the temperature.[8]

H_2SO_4 may be produced on ice (or water) surfaces and also on mineral dust surfaces[19] through adsorption and hydrolysis of gas phase SO_2 or SO_3. Regarding the latter species, the inverse reaction, the dissociation $H_2SO_4 \rightarrow SO_3 + H_2O$ due to an overtone OH stretch excitation of H_2SO_4, has been studied theoretically.[20] However, while the association is exothermic, the dissociation is strongly endothermic, and we did not observe this dissociation mechanism in our work. Recent experimental work has shown that the adsorption of acids, including H_2SO_4 and HCl, on atmospheric mineral dust particles acts to inhibit ice nucleation at moderate humidities.[21] In our work, we hope to shed some light on this issue.

Recent computational studies of H_2SO_4 dissociation include those of Hammerich et al. on this process in both liquid water[22] and at the air-water interface.[23] As reviewed in ref. 23, simulations of a single H_2SO_4 molecule in water clusters show that only 3–4 waters are required for the first deprotonation (see refs. 24 and 25 and additional references in ref. 23 and also refs. 26–29), resulting in the contact ion pair (CIP) $HSO_4^- \cdots H_3O^+$. The second deprotonation requires further solvation, a minimum of 6 waters, resulting in the dicontact ion pair of $H_3O^+ \cdots SO_4^{2-} \cdots H_3O^+$, although this structure is about 8 kcal/mol higher in energy than the most stable structure which is a solvent-separated ion pair (SSIP) involving HSO_4^- and H_3O^+, separated by at least one H_2O, and this is the trend for H_2SO_4-water clusters with up to 9 waters, at which point the doubly deprotonated structure is only about 1 kcal/mol higher in energy.[30] In that study of H_2SO_4 and 6–9 waters, in the cases where the doubly deprotonated structures were observed, SO_4^{2-} was found to participate in about 6 H-bonds with the water molecules.[30] Hammerich et al.[22] studied H_2SO_4 in liquid water and found that as expected experimentally, about 30% of the time double deprotonation occurred. This requires full solvation of the resulting sulfate by surrounding waters and/or hydroniums, and thus is more difficult to achieve at a surface.

Hynes, Bianco, and coworkers,[27–29] have theoretically modeled H_2SO_4 interacting with water ice surfaces. They determined that at the interface where H_2SO_4 is only partially solvated, the likelihood of deprotonation is very sensitive to both solvation and temperature.[28]

Silicon dioxide is one of the most common oxides in the crust of the earth and in the atmospheric boundary layer and in the form of dust in the troposphere, forming 60% of dust particles.[19,31] Silica is also present in built environments as glass or other building materials. Such urban surfaces, including indoor surfaces, often facilitate reactions.[32] In the boundary layer and troposphere, most of the SiO_2 is in the form of sand, or quartz, with α-quartz being the allotrope most prevalent at ordinary temperatures and pressures. Upon cleaving, the (0001) surface is a low energy surface that is commonly exposed. Even under low humidity conditions, the freshly-cleaved surface chemisorbs ambient water, and forms hydroxyl groups in the form of silanols (–SiOH) on the surface.[31] The hydrophilic silanols in turn physisorb water molecules.[31,33] The physisorbed water may be patchy, forming a submonolayer, or may form multiple layers. Under normal to dry conditions of about 20% humidity and 296 K, a full monolayer may form.[34] The water layers closest to the silica surface are highly ordered and form a tessellation ice-

type structure (ice XI,[35] a form of proton-ordered ice) on the surface, and such ices are of interest in their own right.[35–40].

The dissociation of an acid molecule on an oxide surface is an example of an atmospherically-relevant, fundamental heterogeneous chemical reaction. Such reactions, occurring in the presence of a ubiquitous water or ice layer,[37,41] determine surface pH, and may also play a role in enabling other reactions, such as those which lead to ozone depletion (see, e.g., ref. 42). In previous work,[43] we used *ab initio* molecular dynamics to examine the dissociation of HCl on the hydroxylated (0001) α-quartz surface. Acid dissociation and subsequent proton hopping on the surface was observed when the surface water coverage was at least 40%. In addition, the special properties of the ordered water monolayer present on quartz (in particular, the lattice mismatch between the water layer and quartz substrate) enhanced the initial ionization and subsequent proton migration.

In the present study, we explore computationally the mechanisms and time scale of the deprotonation of H_2SO_4 on the (0001) α-quartz surface covered by a water monolayer. The monolayer regime is of interest for low to moderate humidity condition present in the atmosphere. In addition, it allows the quartz surface to exert effects on the ionization process. For the most part, we have not considered multiple layers of water since at these temperatures the subsequent layers quickly begin to resemble the liquid-vapor interface,[44,45] and H_2SO_4 at the vapor-liquid interface has been studied previously.[8,10–18,23] We employ *ab initio* molecular dynamics (AIMD), using density functional theory (DFT),[46,47] for computing the forces "on the fly".[48,49] AIMD simulations can provide an unbiased, atomic-level view of the detailed mechanisms and time scales of chemical reactions.

2 Systems and methods

The same model and techniques were used as in our previous work on HCl.[43] Additional details can be found there and in the Supporting Information of that work. The silica model[44,45] representing the (0001) face of hydroxylated α-quartz consisted of a periodic tetragonal slab with dimensions *xyz* of $9.820 \times 8.504 \times 32.165$ Å^3 (1 Å = 10^{-10} m), with 6 O-Si-O layers, thus leaving a vacuum of about 21 Å between periodic images in the *z*-direction. Both the bottom and top surfaces were fully hydroxylated. The top surface was used to examine reactivity. It contained 8 silanol groups (OH density of 9.6 OH/nm^2). The surface is covered by an ordered monolayer of physisorbed water in the low energy H-down configuration. Three possibilities exist for this monolayer, differing by overall rotations of 120°. They are close in energy (see the ESI and Fig. S1†). As in ref. 43, we use the lowest energy isomer water adlayer. The system is shown in Fig. 1.

The geometry optimizations and the *ab initio* Born-Oppenheimer molecular dynamics (BOMD) simulations were performed at the Γ-point using the QUICKSTEP module within the CP2K package,[50] with the nuclei treated as classical particles. The DFT BLYP[51,52] exchange-correlation functional was used, supplemented by the dispersion correction of Grimme[53] (BLYP-D, using the D2 version of the dispersion correction). We have carefully validated the theory level used (the DFT functional, including the dispersion correction; the basis set; and also *k*-point convergence through use of a larger system size) for correctly recovering the geometry of our system and also the water-surface adhesion energy (see the ESI and Figs. S2-S3†and Tables S1-S2†). Furthermore, BLYP-D has been demonstrated to work well for aqueous systems[54] and for the quartz-water interface.[43–45] The basic procedure in our simulations was the same as in our previous work: Geometry optimization, equilibration in the canonical (NVT) ensemble (3 ps duration, with a 0.5 fs time step), and finally addition of an H_2SO_4 molecule above the surface and calculation of the production trajectories in the microcanonical (NVE) ensemble (5 to 10 ps duration each, with a 0.4 fs time step).

We computed a total of 24 such trajectories to study the acid dissociation dynamics. In all trajectories (with the exception of the last trajectory which studied the second deprotonation), H_2SO_4, in its lowest energy (*trans*) configuration, was placed 3.5–4.5 Å above the wet quartz surface and allowed to fall unto the surface, being steered only by interactions with the surface. 13 trajectories used a double-zeta valence polarization (DZVP) basis set in combination with the appropriate GTH pseudopotential,[55] and were performed at 250 K. Two trajectories were computed using the triple-zeta valence doubly polarized (TZV2P) basis set. The results (geometries, mechanisms, time scales, and spectroscopic signatures) were similar, justifying the use of the smaller basis set for the majority of the calculations. To examine system size and H_2SO_4 coverage effects, a single H_2SO_4 molecule was also allowed to interact with a larger wet quartz surface, one that was doubled in both lateral dimensions. Two trajectories were computed with this larger system. This larger system was also used to examine the second deprotonation when an additional layer of water was allowed to coadsorb. The H_2SO_4:H_2O ratios (H_2SO_4 molarities) of our small system, large system, and large system with a second water layer are thus 1:8 (4.5 M), 1:32 (1.5 M), and 1:64 (0.8 M), respectively. The effect of increasing the temperature was examined by computing two trajectories each at 273, 300, and 330 K. Once H_2SO_4 impacted on the surface, the temperature of the system increased. The increase was correlated with the number of H-bonds formed between H_2SO_4 and surface waters, rather than with deprotonation.

3 Results and Discussion

3.1 First deprotonation

3.1.1 Mechanisms. Fig. 2 shows snapshots from the deprotonation of H_2SO_4 in a typical trajectory at 250 K, and Fig. 3 shows changes in time for this process of the relevant bond lengths and Mulliken partial charges of the participating atoms. Fig. 2(a) and (b) show the starting configuration, followed by the presence of an H_2SO_4 donor H-bond to an H-down (WII) water molecule at 0.86 ps. Following the deprotonation at 0.92 ps, the CIP is shown at 0.97 ps in Fig. 2(c). Note that just prior to the deprotonation, 4 H-bonds link the H_2SO_4 molecule to surface water molecules: H_2SO_4 donates one H-bond while its two oxygens closest to the surface accept three H-bonds from other surface water molecules (see Table S3† for details). The CIP stage is relatively short-lived in this (and in all the deprotonating trajectories), here lasting only until 1.11 ps (CIP duration: ≈ 0.2 ps). The majority of the deprotonating trajectories quickly undergo additional proton hopping via the Grotthuss migration of the proton defect (or proton transfer, PT). The SSIP is shown in Fig. 2(d) at 1.32 ps. HSO_4^- has now shifted configuration somewhat and is accepting H-bonds from water molecules but is not in direct contact with H_3O^+ (we nearly always observed the Eigen structure H_3O^+ rather then the Zundel structure $H_5O_2^+$). Note that H_3O^+ has broken its acceptor H-bond to the underlying silanol (SiOH) prior to this proton transfer. This facilitated the PT by allowing the H_3O^+ to be in its preferred H-bonding state, where it donates its three hydrogen bonds to neighboring water molecules (the so-called DDD H-bonding state).

At 300 K, with the exception of faster deprotonation at the higher temperature, the mechanisms were similar. See the Figs. S4 and S5† which can be compared to Figs. 2 and 3, respectively.

In the six trajectories at 250 K which did not deprotonate, the H_2SO_4 molecule in four cases landed on the surface as a *cis* or *cis*-like rotamer,[56] in a double hydrogen donor configuration, for which H_2SO_4 deprotonation is not favored (see Table S3†). However, in one such case, we observed a short-lived deprotonated species involving a proton wire mechanism where the water molecules allowed a transfer of one of the H_2SO_4 protons from its initial H_2SO_4 oxygen to a different one. The process was completed within about 0.3 ps, in the period 0.56–0.91 ps (see Table S3 and Fig. S6† for details). Proton wire processes are common, and such a process has been observed in a simulation of H_2SO_4 in liquid water in ref. 22.

The remaining three non-deprotonating trajectories were the ones where H_2SO_4 did not establish sufficient H-bonds with the surface waters. As Table S3† shows, the minimum number of H-bonds required for deprotonation is three. This is consistent with earlier computational work (energy minimizations at 0 K) on H_2SO_4 in water clusters[25,26] where it is known that three waters (forming a total of three H-bonds with the H_2SO_4) are needed for the CIP form to be a local minimum (five waters are required for this to be a global minimum). Our results are in broad agreement with those of Re et al.[25] who also found in their study of $H_2SO_4\cdots(H_2O)_{n=1-5}$ that the low energy configurations where both H_2SO_4 hydrogens were donated in the same direction to water molecules did not deprotonate (and were also higher in energy than those situations where only H_2SO_4 hydrogen was donated, leading to deprotonation). However, comparisons to 0 K geometry optimizations of clusters, while useful, are not always relevant for judging the feasibility of deprotonation of a micro-solvated acid molecule at a surface at finite temperature. See the ESI† for further discussion.

3.1.2 Time distribution and yield. Beyond the analysis of mechanisms of first deprotonation of H_2SO_4, our trajectories may be used for additional insights into time scales, protonation yields, and the deprotonation rate. While the statistics are insufficient for definitive quantitative conclusions, we estimate that our study can yield some qualitative and semi-quantitative conclusions.

Since similar mechanisms and deprotonation times were observed for the trajectories calculated using the TZV2P basis set and the larger system (two trajectories each) as for the thirteen trajectories calculated using the DZVP basis set and the small system, all seventeen trajectories at the nominal temperature of 250 K were considered together as an ensemble with an actual average temperature of 263 K (see the ESI and Table S3† for details) in order to estimate the average deprotonation time t_{avg} or equivalently the deprotonation rate $k = 1/t_{avg}$. Eleven of the trajectories were observed to deprotonate within the simulation time of 5–10 ps, with dissociation times in the range 0.38–4.63 ps. Six trajectories did not deprotonate. In three of these, H_2SO_4 landed on the surface in a double hydrogen donor configuration, and in the other three H_2SO_4 was not sufficiently solvated by surface water molecules. This is in agreement with earlier work on H_2SO_4 in water clusters[25,26] where it was observed that a minimum of four waters forming H-bonds are needed for H_2SO_4 deprotonation. The mean dissociation time, 1.1 ps, is a lower limit. Although the statistics are small, with the assumption that the trajectories constitute an ensemble of similarly prepared systems, a better estimate for t_{avg} can be obtained by histogramming the dissociation times. Fig. 4(a) and (b) display the differential of HSO_4^- production, and of the integrated behavior of HSO_4^- production and H_2SO_4 decay/deprotonation times, respectively. The deprotonation or equivalently the time dependence of the H_2SO_4 population decay can be approximately modeled by an exponential, with fractional population

$N(t)/N_0 = \exp(-kt)$, where N_0 = 17. A fit to the cumulative decay data yields k = 0.4 ps^{-1} or t_{avg} = 2 ps. Since our sampling of trajectories has not been extensive, it is better to be less quantitative and to conclude that the average dissociation time is in the range of a few ps.

3.1.3 Arrhenius behavior of deprotonation rate. Two trajectories were computed for each of the higher temperatures of 273, 300, and 330 K. At each temperature, only one of the two trajectories was observed to undergo H_2SO_4 deprotonation (within the 5 ps duration of the trajectories). The starting configurations in these trajectories were nearly identical to corresponding trajectories at 250 K. In addition, the deprotonation mechanisms were observed to be similar. The deprotonation rate approximately followed Arrhenius behavior, considering the few temperatures/trajectories considered and the error bars that should thus be associated to each point (see the ESI and Fig. S7† for details).

3.1.4 Proton migration and disordering of the surface structure. Previously, we found that proton migration initiated by the deprotonation of HCl on the wet quartz surface causes disordering of the initially highly-ordered water layer,[43] in agreement with what has been seen for HCl on neat ice Ih.[57,58] The same disordering occurs during the deprotonation of H_2SO_4 on wet quartz. In Fig. S8 and S9†, we present, respectively, the g_{OO} and g_{OH} radial distribution functions (RDFs), and the orientational distribution functions, of the water adlayer molecules during successive portions of the trajectory. The increasing disorder with time is clearly evident as the original narrow ice-like distributions (and ordered-water distributions with the two water population types) broaden and come to resemble those of liquid water (and non-oriented water) as the system arrives at the SSIP stage.

3.1.5 Spectroscopic signatures of ionization. For the purpose of predicting the signatures of ionization, as in ref. 43 we have computed the spectroscopic signatures in the form of the power spectrum or velocity density of states (VDOS; see e.g., refs. 59 and 60). The VDOS provides all anharmonic vibrational modes of the system, but does not take into account selection rules for the intensity of the bands. Since the purpose is to compare with experimental studies using surface sensitive techniques (such as the existing VSFG experiments of Shen[61–63] and Allen[64] on similar but not identical systems), we have computed the VDOS for the subsystems at the surface of the slab. Fig. 5(a) and (b) show the signatures at 250 K in the critical O-H stretch region of the water layer without H_2SO_4 (or at 0.00 ps prior to the addition of H_2SO_4) and of the water layer with deprotonated H_2SO_4 in the relatively long-lived SSIP state (1.11–7.07 ps), respectively. The water layer and water layer with dissociated H_2SO_4 signals and the changes in the signals upon H_2SO_4 deprotonation are typical of all the dissociating trajectories, including those using the TZV2P basis set and the larger system size, and also, with some variation, of those at the increased temperature of 300 K (see the ESI and Fig. S10†). Including the immediate subsurface hydroxyl or silanol groups in the calculation does not alter the spectral signatures.

Fig. 5(a) shows the expected two peaks in the water layer signal due to the two populations of water molecules on the quartz surface. The so-called "ice-like" and "water-like" peaks at about 3200 and 3400 cm^{-1} are due to the WI (in-plane waters) and WII (H-down waters), respectively (see also ref. 43 for a more extensive discussion). This signal can be compared with that of the water layer with HSO_4^- in the form of the long-lasting SSIP shown in Fig. 5(b). The signals of various relevant free molecules or groups are also shown in panel (a) and can be compared to their counterparts within the water layer plus HSO_4^- shown in panel (b).

Comparing Fig. 5(a) and (b), it is seen that the disordering upon deprotonation and especially proton migration merges and shifts the water layer signal peaks. The presence of the hydronium continuum is also visible. However, unlike in the previous study of HCl ionization,[43] the attachment of H_2SO_4 to water is more energetic than that of HCl. The additional energy raises the system temperature sufficiently and eventually frees waters within the layer and generates a weak signal at about 3700 cm^{-1} corresponding to water with free or dangling OH, consistent with the snapshots (see Fig. 2) and in the measures of large water layer disordering seen in Fig. S8 and S9†. Most importantly, the (single) H_2SO_4 deprotonation is indicated by the presence of intensity due to the O-H stretch in HSO_4^-, which is visible at about 3600 cm^{-1}.

We note that it is also possible to study H_2SO_4, HSO_4^-, and SO_4^{2-} in aqueous environments using VSFG in the lower wavenumber region of 1000–1350 cm^{-1} corresponding to the S-O stretch, see, e.g., refs. 13 and 18. Then the ratios of populations of the various species can be observed directly in the spectrum.

3.2 Second deprotonation

It is of interest to observe the second deprotonation of H_2SO_4. Initially, using our system, this was not seen spontaneously, which is not surprising since it is difficult to sufficiently solvate the H_2SO_4 or HSO_4^- on a surface so as to achieve the required number of H-bonds with neighboring waters. A cluster study[30] has shown that the minimum number of H-bonds is six while we have managed to obtain only five H-bonds in our trajectories (see Table S3†).

Ab initio calculations[65] predict that atmospheric H_2SO_4 may combine with water in a 1:1 or 1:2 ratio at 298.15 K and 45% relative humidity. Thus, we initially attempted to observe the second deprotonation by replacing H_2SO_4 above

the surface (large surface used) with H_2SO_4 presolvated with two or three waters. The $H_2SO_4\cdots(H_2O)_{n=2,3}$ clusters underwent a single deprotonation, forming an $HSO_4^-\cdots H_3O^+$ CIP, prior to interacting with the wet quartz. Upon landing, this state is maintained, with neither additional PT nor additional deprotonation, at least over the duration of our simulations.

However, another coadsorption scenario is possible: adsorption of many waters, for example, a full monolayer, on top of the $HSO_4^-\cdots H_3O^+$ wet quartz system. Thus, one supplementary trajectory (duration of 1.92 ps) was generated from the endpoint of a trajectory where H_2SO_4 had undergone a single deprotonation (see Table S3† for details).

3.2.1 Mechanisms. Fig. 6(a) and (b) show the top and side views of the doubly deprotonated system. The first proton defect has migrated, and forms a distant SSIP to the SO_4^{2-}. Its presence in the second water layer, at the air-water interface allows it to achieve the preferred H_3O^+ state, forming an 'oxygen up' DDD structure with surrounding water molecules, thereby lowering the overall energy. Meanwhile, the second proton defect has formed an $H_3O^+\cdots SO_4^{2-}$ CIP.

As noted, in the singly dissociating trajectories, the proton defect always moved in the same direction (to the right in our figures). The identical deprotonation direction was also observed in the earlier study of deprotonation of HCl on the same surface. In Fig. 6, both proton defects have also shifted in the same direction. This is unlike the case seen in cluster studies,[30] where in the cases of double deprotonation CIPs were formed with the H_3O^+ molecules on opposite sides of SO_4^{2-}. This effect of the quartz surface will be explored in future work.

4 Concluding remarks

Our main finding, is that just as does HCl, H_2SO_4 readily undergoes a first deprotonation on the wet quartz surface, forming HSO_4^- and H_3O^+. Most trajectories were observed to dissociate within 1 ps, and we have estimated an average deprotonation time of 2 ps at 263 K. In agreement with previous studies of H_2SO_4 in aqueous environments, the main determinant of deprotonation is the degree of solvation of H_2SO_4 by neighboring water molecules. The initial deprotonation is followed by migration of the proton defect through the water layer via the Grotthuss mechanism, disordering the water layer. Our calculated VDOS spectral signatures show the presence of the hydronium continuum. However, unlike with HCl, the presence of the O-H stretch in HSO_4^- leads to an additional weak shoulder in the spectrum. Another dissimilarity is that the more energetic interaction of H_2SO_4 with the water layer disorders the layer sufficiently that now water molecules with free O-H are present and can contribute to the vibrational spectrum. The second deprotonation of H_2SO_4 may occur provided that additional waters are available to more fully solvate the bisulfate anion. We deposited a second water layer in order to achieve such a state.

With regard to atmospheric chemistry implications of our research, the favored ionization of acids on wet hydroxylated quartz surfaces and the rapid, few picosecond time scale for the process observed in this work and in ref. 43 implies that the pH value of such surfaces can be very low. The ionization requires that the surface be wetted by about a monolayer (or more) of physisorbed water. Such a layer will be present even at low relative humidity. As mentioned, experimentalists have observed that the adsorption of acids on atmospheric mineral particles inhibit ice nucleation,[21] which is thought to be due to disordering of the lattice. The ordered water layers at water/mica interfaces were reduced at molarities of sulfuric acid equal to 0.5 M and vanished at 5 M.[21] We observed a similar disordering in our study. Our work indicates that the reason for this disordering is the proton migration initiated by the acid ionization.

Acknowledgements

We are grateful to Finland's IT Center for Science Ltd. (CSC) for providing computational resources. We thank the Academy of Finland for its support through the FiDiPro and Lastu programs. RBG additionally acknowledges the Israel Science Foundation (Grant 172/12) and the US National Science Foundation (Grant 0909227). MPG acknowledges HPC-Europa, the Institut Français in Helsinki, the FiDiPro program, and the Fond international of UEVE for funding. GM would like to acknowledge discussions with Sampsa Riikonen.

References

1 B. J. Finlayson-Pitts and J. N. Pitts, *Chemistry of the Upper and Lower Atmosphere: Theory, Experiments, and Applications*, Academic Press, San Diego, CA, USA, 2000.
2 R. P. Wayne, *Chemistry of Atmospheres: An Introduction to the Chemistry of the Atmospheres of Earth, the Planets, and their Satellites*, Oxford University Press, Oxford, 2000.
3 M. Kulmala, *Science*, 2003, **302**, 1000–1001.
4 IPCC, Climate Change 2007: The Physical Science Basis, Cambridge University Press, Cambridge, UK, and New York, NY, USA.
5 J. J. Blackstock, D. S. Battisti, K. Caldeira, D. M. Eardley, J. I. Katz, D. W. Keith, A. A. N. Patrinos, D. P. Schrag, R. H. Socolow and S. E. Koonin, Climate Engineering Responses to Climate Emergencies (Novim, 2009), archived online at: http://arxiv.org/pdf/0907.5140.
6 G. C. Hegerl and S. Solomon, *Science*, 2009, **325**, 955–956.
7 G. Rubasinghege and V. H. Grassian, *Chem. Commun.*, 2013, **49**, 3071–3094.
8 A. M. Margarella, K. A. Perrine, T. Lewis, M. Faubel, B. Winter and J. C. Hemminger, *J. Phys. Chem. C*, 2013, **117**, 8131–8137.
9 D. A. Knopf, B. P. Luo, U. K. Krieger and T. Koop, *J. Phys. Chem. A*, 2003, **107**, 4322–4332.

10 C. Radüge, V. Pflumio and Y. R. Shen, *Chem. Phys. Lett.*, 1997, **274**, 140–144.
11 M. J. Shultz, C. Schnitzer, D. Simonelli and S. Baldelli, *Int. Rev. Phys. Chem.*, 2000, **19**, 123–153.
12 S. Gopalakrishnan, D. Liu, H. C. Allen, M. Kuo and M. J. Shultz, *Chem. Rev.*, 2006, **106**, 1155–1175.
13 T. Miyamae, A. Morita and Y. Ouchi, *Phys. Chem. Chem. Phys.*, 2008, **10**, 2010–2013.
14 T. Ishiyama, A. Morita and T. Miyamae, *Phys. Chem. Chem. Phys.*, 2011, **13**, 20965.
15 T. Ishiyama and A. Morita, *J. Phys. Chem. C*, 2011, **115**, 13704–13716.
16 A. M. Jubb and H. C. Allen, *J. Phys. Chem. C*, 2012, **116**, 13161–13168.
17 C. M. Johnson and S. Baldelli, *Chem. Rev.*, 2014.
18 T. Ishiyama, T. Imamura and A. Morita, *Chem. Rev.*, 2014.
19 C. R. Usher, A. E. Michel and V. H. Grassian, *Chem. Rev.*, 2003, **103**, 4883–4940.
20 Y. Miller and R. B. Gerber, *J. Am. Chem. Soc.*, 2006, **128**, 9594–9595.
21 Z. Yang, A. K. Bertram and K. C. Chou, *J. Phys. Chem. Lett.*, 2011, **2**, 1232–1236.
22 A. Hammerich, V. Buch and F. Mohamed, *Chem. Phys. Lett.*, 2008, **460**, 423–431.
23 A. D. Hammerich and V. Buch, *J. Phys. Chem. A*, 2012, **116**, 5637–5652.
24 H. Arstila, K. Laasonen and A. Laaksonen, *J. Chem. Phys.*, 1998, **108**, 1031–1039.
25 S. Re, Y. Osamura and K. Morokuma, *J. Phys. Chem. A*, 1999, **103**, 3535–3547.
26 K. R. Leopold, *Annu. Rev. Phys. Chem.*, 2011, **62**, 327–349.
27 R. Bianco and J. T. Hynes, *Theor. Chem. Acc.*, 2004, **111**, 182–187.
28 R. Bianco, S. Wang and J. T. Hynes, *J. Phys. Chem. B*, 2005, **109**, 21313–21321.
29 R. Bianco and J. T. Hynes, *Acc. Chem. Res.*, 2006, **39**, 159–165.
30 C.-G. Ding and K. Laasonen, *Chem. Phys. Lett.*, 2004, **390**, 307–313.
31 A. Rimola, D. Costa, M. Sodupe, J.-F. Lambert and P. Ugliengo, *Chem. Rev.*, 2013, **113**, 4216–4313.
32 J. D. Raff, B. Njegic, W. L. Chang, M. S. Gordon, D. Dabdub, R. B. Gerber and B. J. Finlayson-Pitts, *Proc. Nat. Acad. Sci. USA*, 2009, **106**, 13647–13654.
33 E. Papirer, *Adsorption on Silica Surfaces*, Marcel Dekker, New York, 2000.
34 A. L. Goodman, E. T. Bernard and V. H. Grassian, *J. Phys. Chem. A*, 2001, **105**, 6443–6457.
35 Y.-W. Chen, I.-H. Chu, Y. Wang and H.-P. Cheng, *Phys. Rev. B*, 2011, **84**, 155444.
36 J. Yang and E. G. Wang, *Phys. Rev. B*, 2006, **73**, 035406.
37 M. A. Henderson, *Surf. Sci. Rep.*, 2002, **46**, 1–308.
38 H. Wang, R. C. Bell, M. J. Iedema, A. A. Tsekouras and J. P. Cowin, *Astrophys. J.*, 2005, **620**, 1027.
39 G. A. Kimmel, J. Matthiesen, M. Baer, C. J. Mundy, N. G. Petrik, R. S. Smith, Z. Dohnálek and B. D. Kay, *J. Am. Chem. Soc.*, 2009, **131**, 12838–12844.
40 G. A. Kimmel, M. Baer, N. G. Petrik, J. VandeVondele, R. Rousseau and C. J. Mundy, *J. Phys. Chem. Lett.*, 2012, **3**, 778–784.
41 P. J. Feibelman, *Phys. Today*, 2010, **63**, 34–39.
42 Z. Liu, C. Siu and J. S. Tse, *Chem. Phys. Lett.*, 1999, **309**, 335–343.
43 G. Murdachaew, M.-P. Gaigeot, L. Halonen and R. B. Gerber, *J. Phys. Chem. Lett.*, 2013, **4**, 3500–3507.
44 M. Sulpizi, M.-P. Gaigeot and M. Sprik, *J. Chem. Theory Comput.*, 2012, **8**, 1037–1047.
45 M.-P. Gaigeot, M. Sprik and M. Sulpizi, *J. Phys.: Condens. Matter*, 2012, **24**, 124106.
46 P. Hohenberg and W. Kohn, *Phys. Rev. B*, 1964, **136**, 864–871.
47 W. Kohn and L. J. Sham, *Phys. Rev. A*, 1965, **140**, 1133–1138.
48 R. Car and M. Parrinello, *Phys. Rev. Lett.*, 1985, **55**, 2471–2474.
49 D. Marx and J. Hutter, *Ab Initio Molecular Dynamics: Basic Theory and Advanced Methods*, Cambridge, New York, 2009.
50 The CP2K developers group, `http://www.cp2k.org/`, 2000-2014.
51 A. D. Becke, *Phys. Rev. A*, 1988, **38**, 3098–3100.
52 C. Lee, W. Yang and R. G. Parr, *Phys. Rev. B*, 1988, **37**, 785–789.
53 S. Grimme, *J. Comput. Chem.*, 2006, **27**, 1787–1799.
54 J. Schmidt, J. VandeVondele, I.-F. W. Kuo, D. Sebastiani, J. I. Siepmann, J. Hutter and C. J. Mundy, *J. Phys. Chem. B*, 2009, **113**, 11959–11964.
55 S. Goedecker, M. Teter and J. Hutter, *Phys. Rev. B*, 1996, **54**, 1703.
56 D. K. Havey, K. J. Feierabend and V. Vaida, *J. Mol. Struct.: THEOCHEM*, 2004, **680**, 243–247.
57 Y. A. Mantz, F. M. Geiger, L. T. Molina, M. J. Molina and B. L. Trout, *J. Chem. Phys.*, 2000, **113**, 10733–10743.
58 Y. A. Mantz, F. M. Geiger, L. T. Molina, M. J. Molina and B. L. Trout, *Chem. Phys. Lett.*, 2001, **348**, 285–292.
59 M.-P. Gaigeot, M. Martinez and R. Vuilleumier, *Mol. Phys.*, 2007, **105**, 2857–2878.
60 M. Thomas, M. Brehm, R. Fligg, P. Vohringer-Martinez and B. Kirchner, *Phys. Chem. Chem. Phys.*, 2013, **15**, 6608–6622.
61 Q. Du, E. Freysz and Y. R. Shen, *Science*, 1994, **264**, 826–828.
62 V. Ostroverkhov, G. A. Waychunas and Y. Shen, *Chem. Phys. Lett.*, 2004, **386**, 144–148.
63 Y. R. Shen and V. Ostroverkhov, *Chem. Rev.*, 2006, **106**, 1140–1154.
64 H. C. Allen, N. N. Casillas-Ituarte, M. R. Sierra-Hernández, X. Chen and C. Y. Tang, *Phys. Chem. Chem. Phys.*, 2009, **11**, 5538–5549.
65 H. Henschel, J. C. A. Navarro, T. Yli-Juuti, O. Kupiainen-Määttä, T. Olenius, I. K. Ortega, S. L. Clegg, T. Kurtén, I. Riipinen and H. Vehkamäki, *J. Phys. Chem. A*, 2014, **118**, 2599–2611.

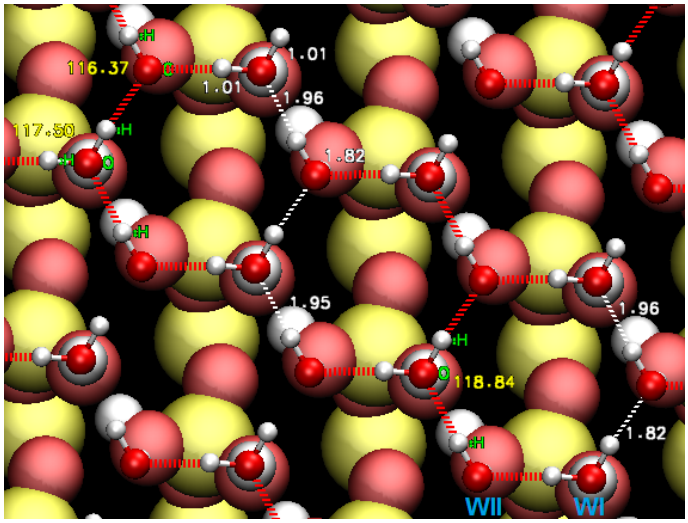

(a) Top view

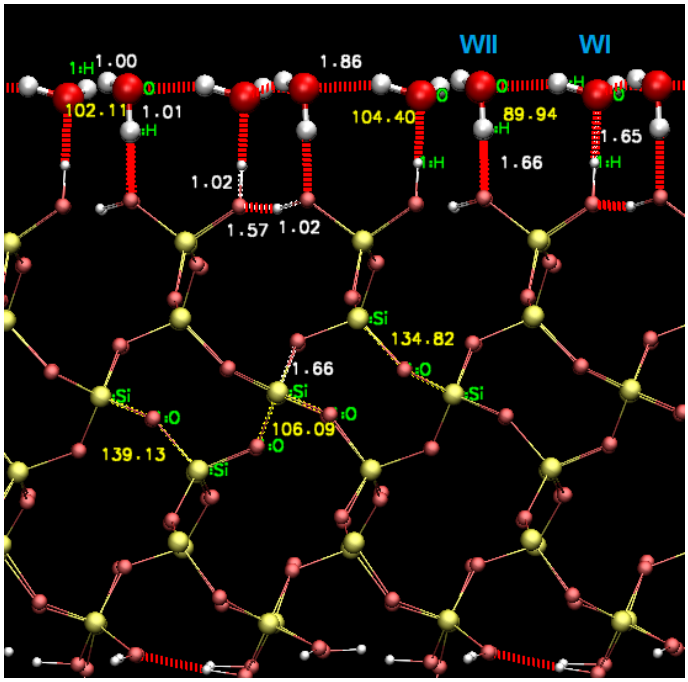

(b) Side view

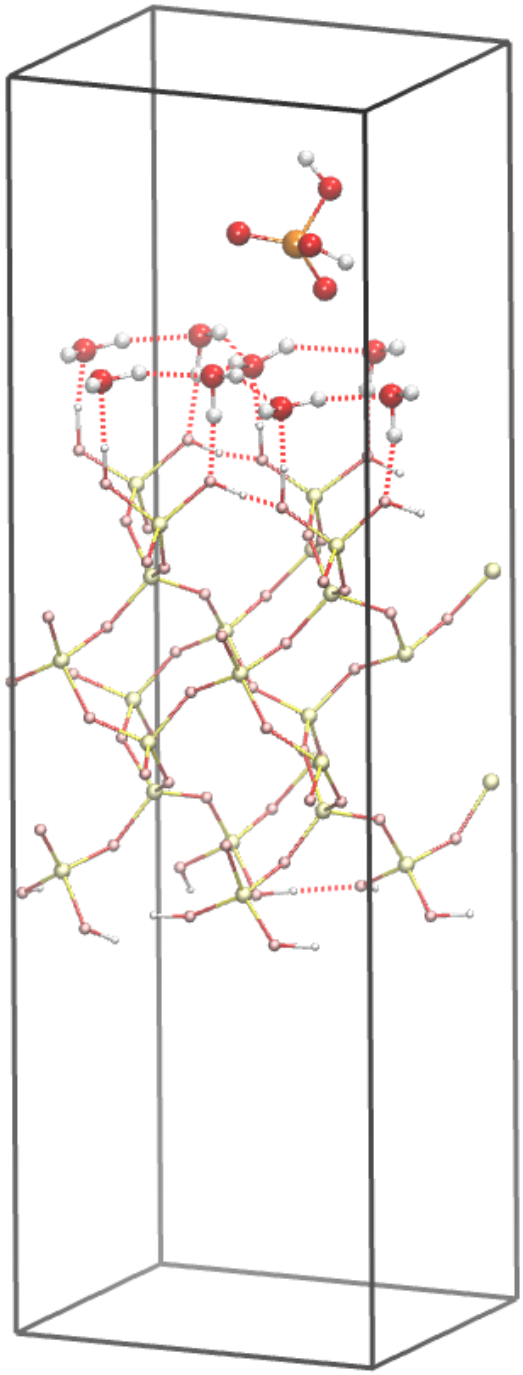

(c) Complete system within simulation box

Fig. 1 (a) Top and (b) side view of the adsorbing surface consisting of the two populations of water molecules (in-plane waters, WI; and H-down waters, WII) physisorbed unto the hydroxylated (0001) surface of α-quartz. Approximately 2.5 unit cells in the plane are shown. H-bonds are not drawn across cell boundaries. (c) View of complete system within the simulation box, with H_2SO_4 in a starting position above the surface.

(a) t = 0.00 ps:
H_2SO_4 released 3.5 Å above the wet quartz surface

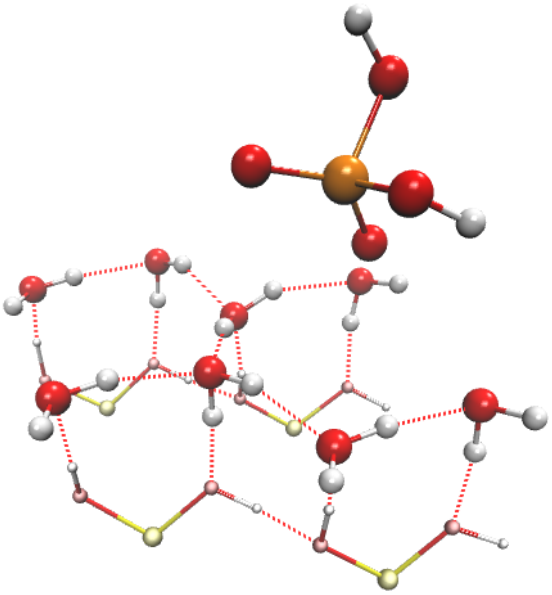

(b) t = 0.86 ps:
$H_2O\cdots H_2SO_4$ H-bond

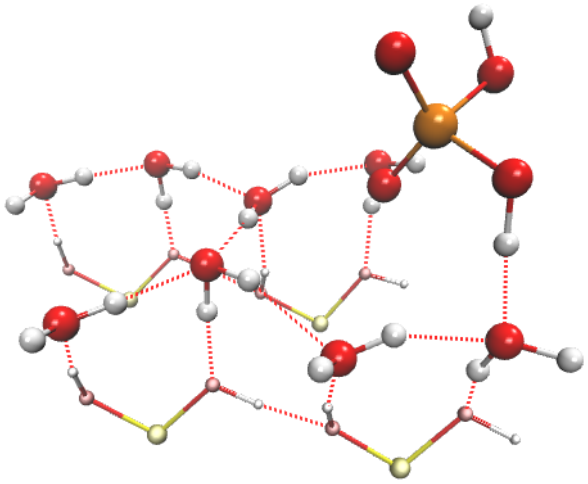

(c) t = 0.97 ps:
Contact Ion Pair $HSO_4^-\cdots H_3O^+$

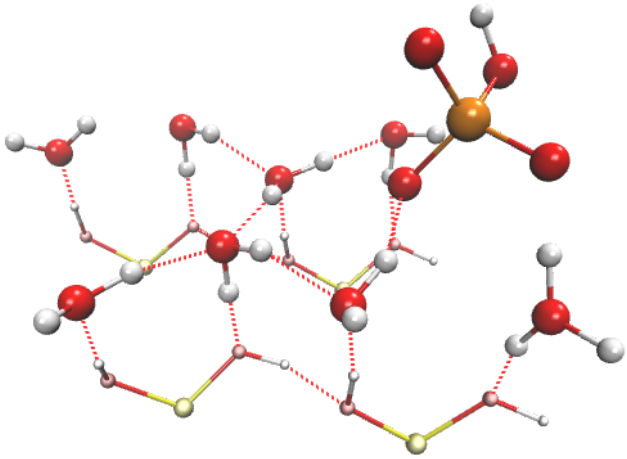

(d) t = 1.32 ps:
Solvent-Separated Ion Pair $HSO_4^-\cdots H_2O\cdots H_3O^+$

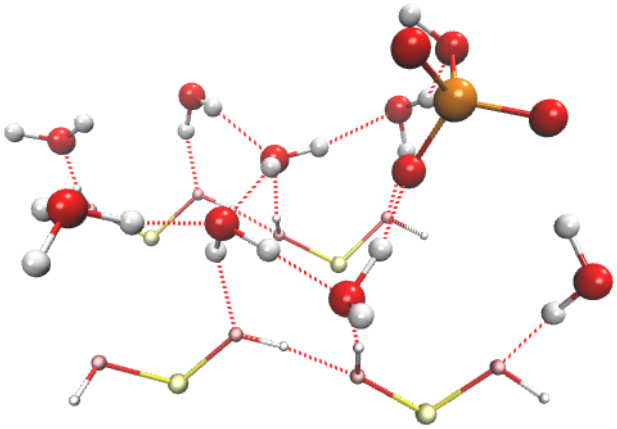

Fig. 2 Snapshots showing the H_2SO_4 first deprotonation and subsequent proton migration at 250 K (perspective view; silanol top layer only shown; sulfur, orange; oxygen, red; hydrogen, white; silicon, yellow). In panel (d) the water molecule to which H^+ has transferred is located across the periodic boundary of the simulation cell, at the left side of the image. The data are from Trajectory 1.

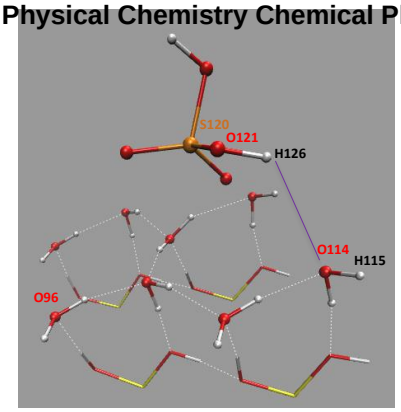

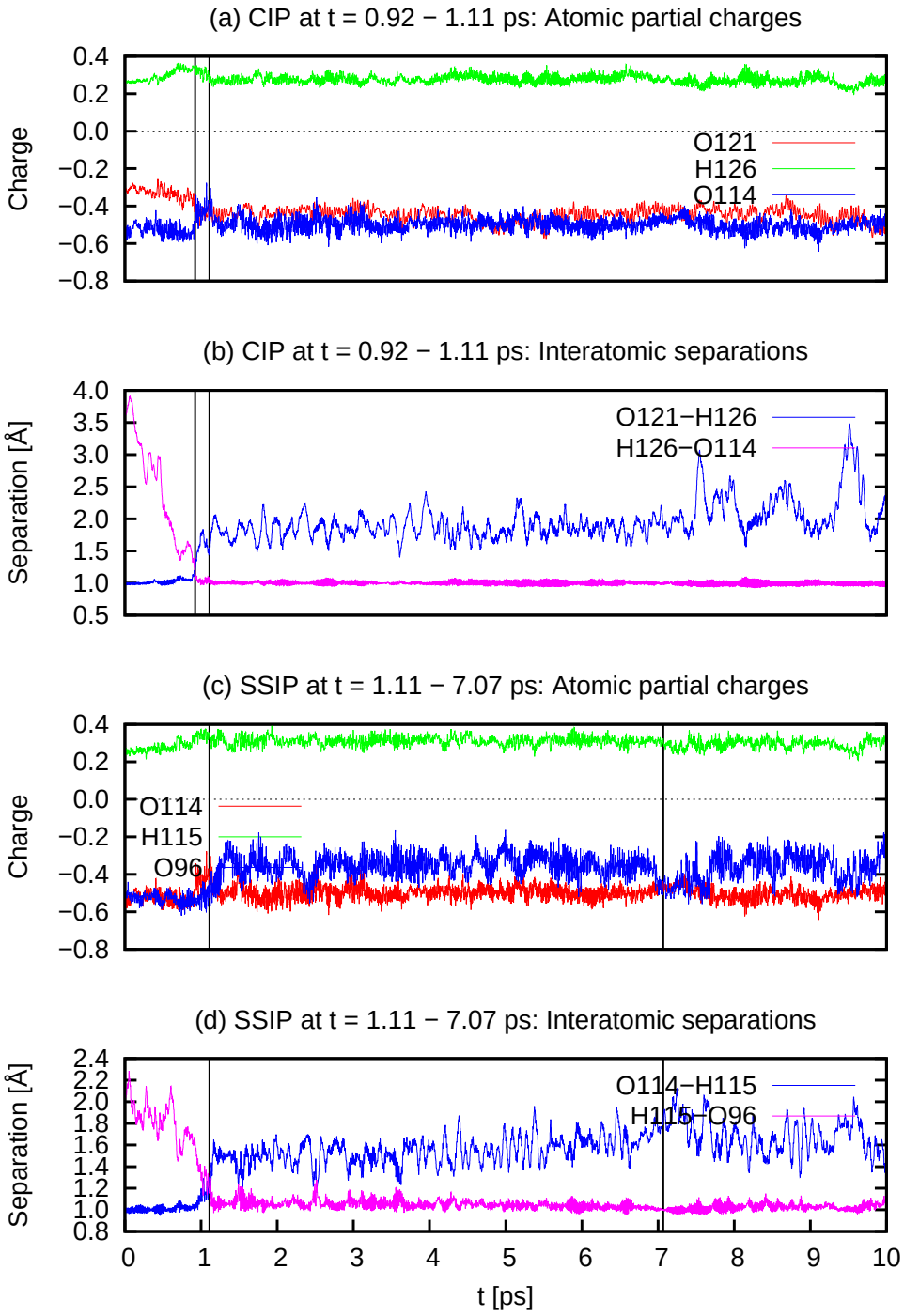

Fig. 3 Interatomic separations and partial Mulliken charges of relevant atoms during the proton migration at 250 K. The snapshot (at t = 0.00 ps) shows the atom labels. The black vertical lines draw attention to relevant time intervals. The data are from Trajectory 1. See also Fig. 2(a)–(d) for geometries.

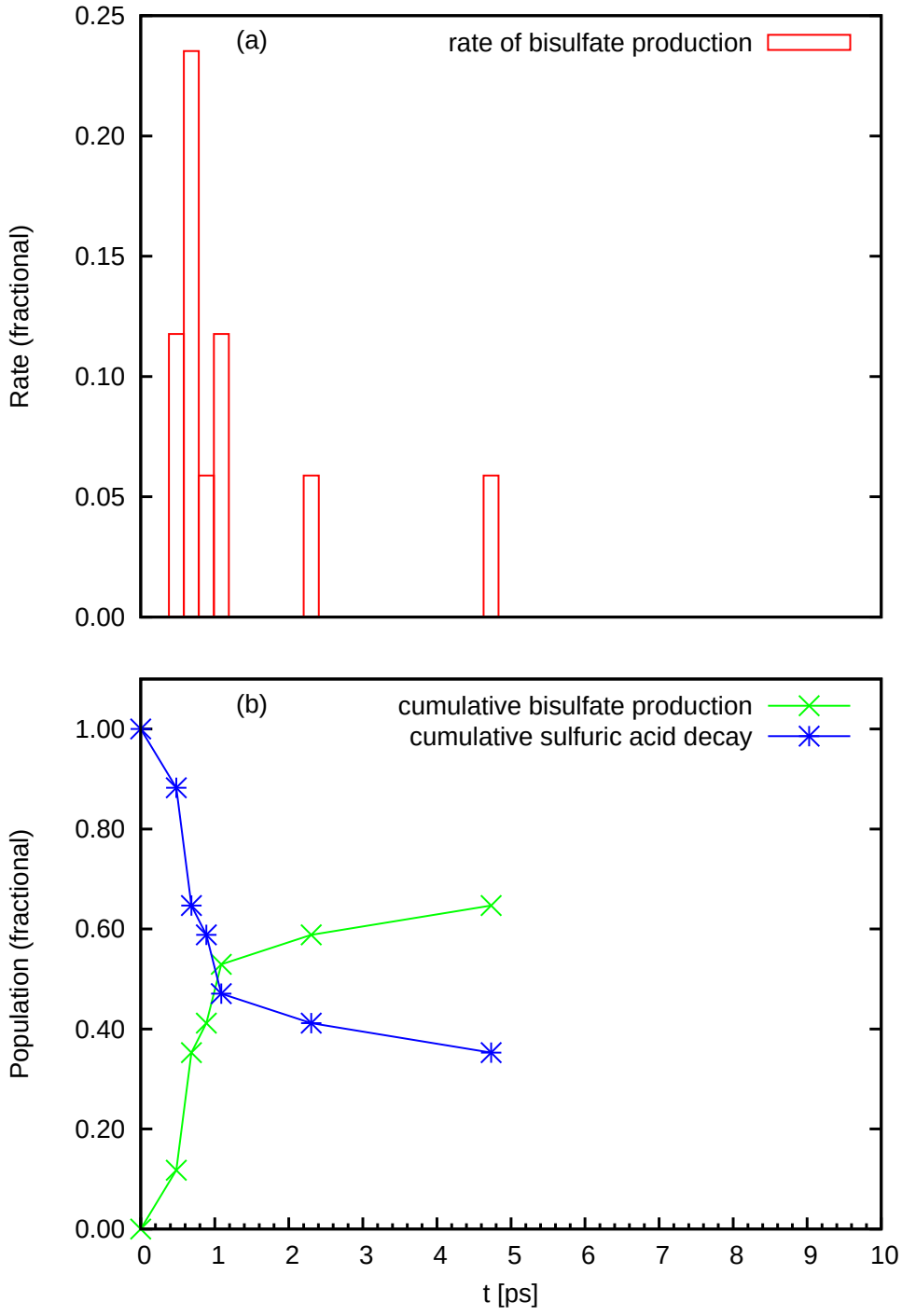

Fig. 4 Time distribution of first proton deprotonation times of sulfuric acid on wet quartz at 250 K. See text for additional details. The data come from 17 trajectories (see Table S3†).

(a) t = 0.00 ps: Before introduction of H_2SO_4 to the surface
(separate 5 ps trajectories)

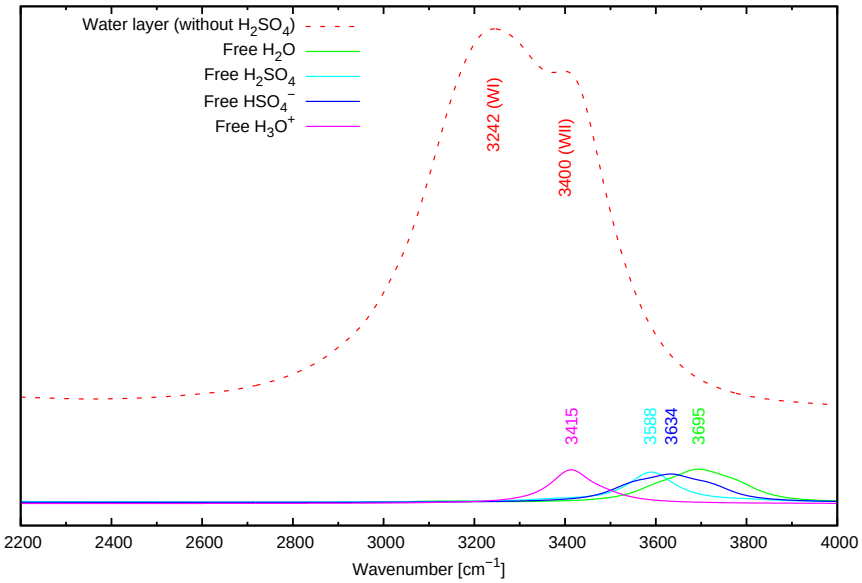

(b) t = 1.11–7.07 ps: After introduction of H_2SO_4
(existence of SSIP $HSO_4^- \cdots H_2O \cdots H_3O^+$)

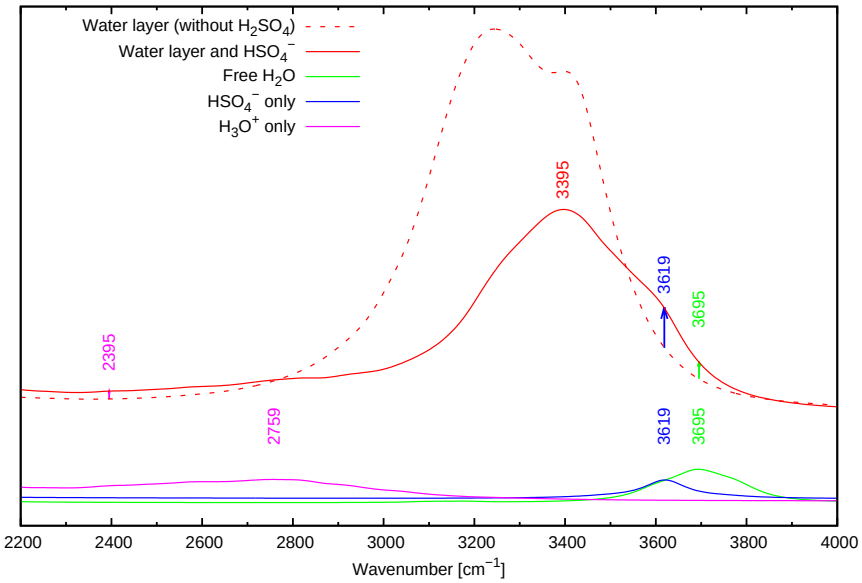

Fig. 5 Vibrational spectra (VDOS) during the proton migration at 250 K. VDOS were computed for the indicated time interval. In panel (b) (red curve), HSO_4^- causes the weak shoulder at about 3620 cm^{-1} (free water OH also contributes in this region), and H_3O^+ causes the small increase in intensity in the broad region at 2800 cm^{-1} and below. The data are from Trajectory 1. See also Fig. 2(a) and Fig. 2(d) for the geometries corresponding to panels (a) and (b), respectively.

(a) Top view

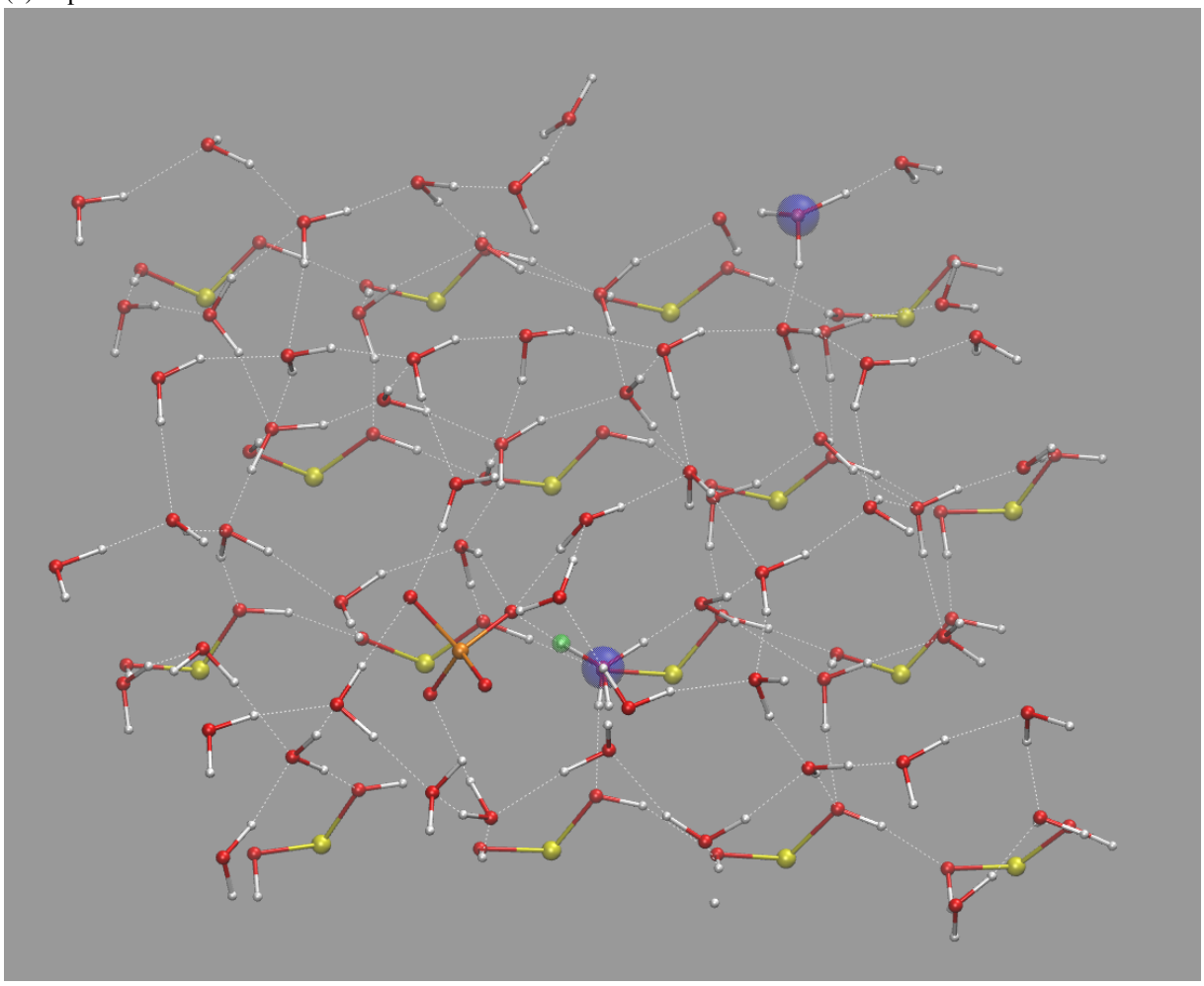

(b) Side view

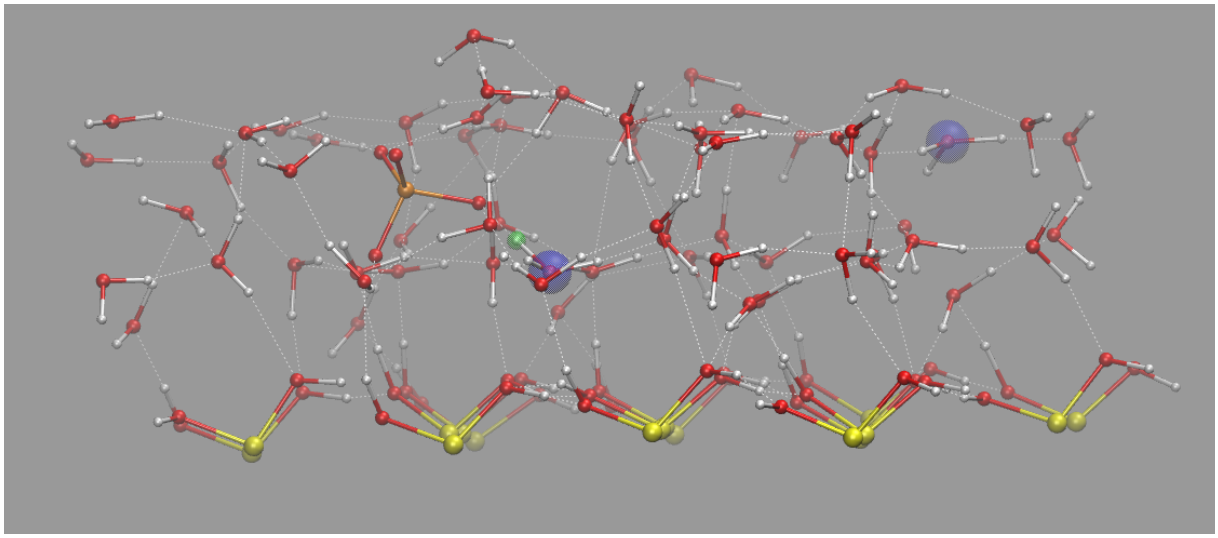

Fig. 6 Final snapshot from the large system, covered by a second layer of water molecules coadsorbed on top of the acid and wet quartz. The second deprotonation has occurred and SO_4^{2-} is present. The first and second H_3O^+ molecules (both highlighted in blue) are, respectively, a distant SSIP, and a CIP, relative to the SO_4^{2-}) molecule. The second detached proton in highlighted in green. The data are from Trajectory 5a, at t = 1.92 ps (see Table S3†).